Journal Pre-proofs

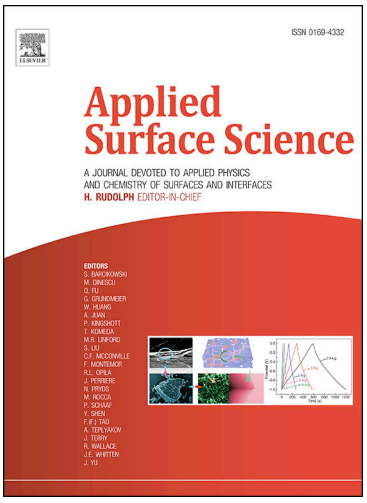

Full Length Article

Bottom-up microwave-assisted seed-mediated synthesis of gold nanoparticles onto nanocellulose to boost stability and high performance for SERS applications

A.C. Marques, T. Pinheiro, M. Morais, C. Martins, A.F. Andrade, R. Martins, M. G. F. Sales, E. Fortunato

PII: S0169-4332(21)01136-3
DOI: https://doi.org/10.1016/j.apsusc.2021.150060
Reference: APSUSC 150060

To appear in: *Applied Surface Science*

Received Date: 25 March 2021
Revised Date: 20 April 2021
Accepted Date: 5 May 2021

Please cite this article as: A.C. Marques, T. Pinheiro, M. Morais, C. Martins, A.F. Andrade, R. Martins, M. G. F. Sales, E. Fortunato, Bottom-up microwave-assisted seed-mediated synthesis of gold nanoparticles onto nanocellulose to boost stability and high performance for SERS applications, *Applied Surface Science* (2021), doi: https://doi.org/10.1016/j.apsusc.2021.150060

Bottom-up microwave-assisted seed-mediated synthesis of gold nanoparticles onto nanocellulose to boost stability and high performance for SERS applications

A. C. Marques[1,2], T. Pinheiro[1], M. Morais[1], C. Martins[1], A. F. Andrade[1], R. Martins[1], M. G. F. Sales[2,3], E. Fortunato[1,*]

[1]CENIMAT|i3N, Departamento de Ciência de Materiais, Faculdade de Ciências e Tecnologia, Universidade NOVA de Lisboa and CEMOP/UNINOVA, Campus da Caparica, 2829-516 Caparica – Portugal

[2]BioMark@UC, Department of Chemical Engineering, Faculty of Science and Technology, Coimbra University, 3030-790, Coimbra, Portugal

[3]CEB – Centre of Biological Engineering, University of Minho, 4710-057 Braga, Portugal

*corresponding author: emf@fct.unl.pt (EF)

Abstract

The development of accurate, reliable, inexpensive and fully recyclable analytical platforms is of utmost relevance to several fields from medical diagnosis to environmental screening. Surface-enhanced Raman spectroscopy (SERS) is a compelling detection method with high specificity and sensitivity. In this work, a microwave-assisted synthesis method was used for fast and uniform in situ growth of gold nanoparticles (AuNPs) onto nanocellulose (NC) membranes, through a seed-mediated process. The as-prepared membranes were fully optimized and its application as SERS platforms was demonstrated. A direct comparison with other cellulose-based substrates showed the superior characteristics of NC such as high mechanical strength, high surface area and lower porous content. An Enhancement Factor (EF) up to ~10^6 was obtained using rhodamine 6G (R6G) 10^{-6} M as probe molecule and a remarkable shelf life of at least 7 months was achieved, with no special storage required. Preliminary results on the detection of label-free spike protein present in SARS-CoV-2 virus are shown, through direct measurements on the optimized SERS membrane. We believe that this work evidences the effectiveness of in situ seed-mediated microwave-assisted synthesis as a fabrication method, the high stability of AuNPs and the superior characteristics of NC substrates to be used as SERS platforms.

Keywords: Microwave-assisted synthesis; Gold nanoparticles; Nanocellulose; SERS: Point-of-care biosensors; COVID-19.

1. Introduction

The novel coronavirus disease (COVID-19) outbreak has reinforced the high demand for fast, reliable, accurate and specific detection techniques. Surface-Enhanced Raman Spectroscopy (SERS) is a powerful analytical method that combines the rich and unique information provided by Raman scattering with the signal amplification supplied by some metallic surfaces. The SERS effect can be explained and divided into two mechanisms: electromagnetic (EM) and chemical (CM) enhancement. EM enhancement contributes for the highest enhancement factors (EF) and arises from the electromagnetic field caused by the Localized Surface Plasmon Resonance (LSPR) of metal nanostructures, such as silver and gold nanoparticles (AgNPs and AuNPs, respectively). CM enhancement has lower EF and is related with charge transfer processes between the analyte and the SERS structures.[1–5]

The advance on nanofabrication tools has expedited the research on the fabrication of SERS platforms using both physical to wet chemical processes. The effectiveness on Raman enhancement is highly dependent on the preparation methods of SERS-active layers. Traditionally, top-down techniques, such as lithography and physical-deposition processes, have been used to fabricate SERS platforms. However, these techniques can be cumbersome, expensive, difficult to scale up and time-consuming.[2,6] Chemical-based processes are affordable, simple, scalable, easily tailored and liable high-throughput. Among the wet chemistry methods, microwave-assisted synthesis uses volumetric dielectric heating, allowing for rapid and uniform heating of the reaction mixture resulting in well-controlled and homogenous products - as compared with its counterpart conventional heating - resulting in a decrease on reaction time by more than one order of magnitude.[2,7–9]

Various SERS platforms have been reported using microwave-assisted synthesis to produce enhancement nanostructures and are mostly based on Ag nanostructures.[1,2,6,7,10–13] Although AgNPs are able to provide the highest Raman enhancements, due to their strong plasmon resonance effect, they are chemically unstable and prone to early oxidation, which can compromise the shelf life of SERS platforms.[14] On the contrary, AuNPs have high chemical

stability, are biocompatible and offer easy functionalization with biomarkers. So, the development of microwave-based fabrication strategies for AuNPs-based SERS platforms is of high relevance. In 2014, Su, S. and colleagues used microwave irradiation to decorate MoS_2 nanosheets with AuNPs.[15] A relative standard deviation (RSD) of around 20% was attained with an EF of 8.2 x 10^5 with 10^{-4} M R6G as probe molecule. Later, a method to prepare Au-graphene-Au dimers and its used for SERS was reported by Ghosh, P. et al., with an EF of around 10^7 with R6G.[16] The method combined microwave-assisted synthesis of a first layer of AuNPs grown in an amino-functionalized Si wafer, transfer of a graphene monolayer from a copper foil to the Au-SiO_2 substrate, followed by microwave growth of the second layer of AuNPs. More recently, Li, H. and co-workers described a method for the microwave synthesis of AuNPs prepared with a magnetic ionic liquid, used as a synergistic enhancer and stabilizing compound, for the detection of clopidol.[17] However, some of the works reported so far require multi-step approaches, relying on expensive substrates and materials in addition to lack of practicality in the measurement regime.

The use of supporting matrices for the Raman enhancement nanostructures offers a higher convenience and higher throughput for SERS measurements and, in some cases, can enhance the Raman signal amplification even further. Many materials have been used as SERS substrates, from conventional glass, silicon wafers to cellulose-based substrates.[13,18–25] Cellulose is an outstanding polymeric material due to its inherent low-cost, lightweight, biocompatibility, recyclability and versatility. It exists in many formats, from the regular office paper to nanoscale formats, such as nanocellulose. Besides the aforementioned cellulose properties, nanocellulose possesses a high mechanical strength and thermal stability and a high surface-to-volume ratio, which can help obtaining SERS platforms with densely packed plasmonic nanostructures, creating the so-called SERS hot-spots.[8,13,24,26–30]

Since the first reports on cellulose as SERS platform in 1984,[31,32] several cellulose-based SERS substrates have been proposed in the literature, with different cellulose formats, nanostructures fabrication strategies and deposition methods.[11,13,14,33–35] Among the deposition methods, in situ synthesis methods[36–40] show benefits since the nanostructures' production and their deposition on the substrate can be done in a single step. This generally leads

to simple and fast SERS platform's fabrication, avoiding, for instance, long immersion times of the substrate onto plasmonic nanoparticles colloidal solutions.[41]

In this work, nanocellulose substrates obtained from *nata de coco* were used for the fabrication of gold-based nanocellulose SERS platforms. The said platforms were produced by the in situ growth of AuNPs onto the nanocellulose substrate with a seed-mediated growth method. Microwave irradiation was employed on the AuNPs synthesis, resulting in a uniform and inexpensive SERS platform with a production time of less than 1 hour. The herein presented SERS platforms were directly compared with other cellulose formats and were fully optimized in terms of AuNPs synthesis procedure and fabrication method attaining an EF up to 10^6 with a high shelf life of at least 7 months. As a proof-of-concept, preliminary results of the detection of the spike protein of SARS-CoV-2 virus are shown, thus demonstrating the potentialities of the developed method for SERS membranes fabrication.

2. Experimental section

2.1. Materials and solutions

Raw *nata de coco* cubes were commercially obtained from Zhen Xin Canned Food. Tetrachloroauric(III) acid ($HAuCl_4.3H_2O$, ≥ 99.9%, Sigma Aldrich), β-D-glucose (≥ 99.9%, Sigma Aldrich), trisodium citrate (Na_3Ct, ≥ 99.9%, Carl Roth), sodium hydroxide (NaOH, LABKEM), rhodamine 6G (R6G, Sigma Aldrich) and phosphate buffered saline pH 7.2 (PBS, BioUltra) were used as received without further purification. Recombinant SARS-CoV-2 spike protein, S1 subunit (230-01101) was purchased from RayBiotech. Distilled water passed through a Millipore water system (ρ = 18.2 MΩ) was used in all experiments.

2.2. Solution-based gold nanoparticles synthesis

A volume of 0.5 ml of a $HAuCl_4$ solution was transferred to a microwave vessel followed by 0.5 ml of a reducing agent (RA) solution and 4.0 ml of distilled water. Two different final concentrations of $HAuCl_4$ were tested, 0.5 and 1.0 mM, and two different reducing agents (RA) were used, Na_3Ct and glucose, at the final concentrations of 2.5 and 5.0 mM. When glucose was used as RA, 60 µl of 1 M NaOH were added to the solution. The prepared vessels were then transferred to a

microwave reactor from CEM Discover, and the parameters were set to 120 ºC, 10 min reaction time at 100 W, with a safe maximum pressure of 280 psi. Prior to use, all glassware was soaked in *aqua regia* (HCl/HNO_3 3:1, v/v) for 24 h and rinsed with Millipore water.

2.3. Preparation of SERS membranes: in situ gold nanoparticles synthesis

The NC membranes were obtained from *nata de coco* cubes, according to the method published by Ferreira, N. et al.[13] Briefly, *nata de coco* cubes previously thoroughly washed and maintained in an ethanol solution, were subjected to a 15 min manual pressing (HeatPress UK, Swing-a-way), followed by a drying process at 40 ºC. Afterwards, the dried membranes were subjected to a 10 ton pressing (Manual hydraulic press, Specac, 15 ton max.) for 2 min, to achieve their final thickness between 40 to 50 µm.

The in situ AuNPs synthesis onto NC membranes (NC@AuNPs) was achieved through a seed-mediated growth method, with the previously optimized concentrations and microwave parameters (1.0 mM $HAuCl_4$ and 5.0 mM Na_3Ct at 120 °C for 10 min at 100 W) resorting to two reaction cycles. In the first cycle, a 2.25 cm^2 NC membrane was incubated (NC_{inc}) for 30 min in the reaction mixture and subjected afterwards to microwave irradiation. Next, the seed-NC membrane was transferred to a freshly prepared reaction mixture and subjected to a second microwave irradiation cycle. After each cycle, the membranes were thoroughly washed under a gentle stream of distilled water to remove unreacted species. The NC_{inc}@AuNPs obtained after the second cycle were allowed to dry at room temperature in a desiccated environment. For SERS performance comparison purposes other membranes were also produced, based on NC membranes without the incubation step (NC@AuNPs), with and without the incubation step with a seedless method and a reaction time of 20 min ($NC_{inc\text{-}20min}$@AuNPs and NC_{20min}@AuNPs, respectively), and based on other cellulosic substrates with the optimized conditions: Whatman paper (WP_{inc}@AuNPs), office paper (OP_{inc}@AuNPs) and cardboard substrate (CB_{inc}@AuNPs).

2.4. Characterization

The optical characteristics of the synthesized AuNPs colloidal solutions were assessed through UV-Vis spectroscopy (Spark® multimode microplate reader, TECAN, Switzerland). Imaging of AuNPs was carried out by transmission electron microscopy (TEM, ThermoFisher Scientific Inc, TITAN C-Twin) operated at 300 kV. The size of the AuNPs was determined by Dynamic Light

Scattering (DLS, AvidNano W130i, USA). The SERS membranes were chemically, structurally and morphologically characterized through X-ray photoelectron spectroscopy (XPS, Kratos Axis Supra, UK) equipped with a monochromated Al Kα radiation (1486.6 eV), X-ray diffraction (XRD, Malvern Panalytical, X'Pert Pro, UK) equipped with a CuKα target and wavelength of 1.5406 Å and Scanning Electron Microscopy (SEM, Carl Zeiss AURIGA FIB-SEM Crossbeam, Oberkochen, Germany), respectively.

2.5. SERS measurements and Enhancement factor calculation

The prepared SERS membranes were individualized into 2 mm^2 squares, for single measurements, to each square a 2 µl drop of analyte was deposited and allowed to dry at RT. SERS spectra acquisition was achieved with a Renishaw inVia Qontor confocal Raman microscope (Gloucestershire, UK) equipped with a Renishaw Centrus 2957T3 detector. Before measurements, the equipment was calibrated with an internal silicon wafer at Raman shift of 520 cm^{-1}. Measurements were performed with a 633 nm laser at 3.2 mW with 10 sec exposure time and 10 accumulations. A 50× Olympus objective lens (N10.6 LMPLAN FL N) was used to focus the laser beam. The SERS EF was calculated using R6G 10^{-6} M probe molecule and determined using equation 1:[42,43]

$$EF = \frac{I_{SERS}}{I_{Raman}} \times \frac{N_{Raman}}{N_{SERS}} \qquad \text{eq. 1}$$

where I_{SERS} and I_{Raman} are the integrated signal intensities of R6G and N_{SERS} and N_{Raman} are the number of R6G molecules deposited on SERS and Raman substrate, calculated by equation 2:

$$N_{SERS/Raman} = N_A \times V \times C_{SERS/Raman} \times \frac{A_{laser}}{A_{SERS}/Raman} \qquad \text{eq. 2}$$

where N_A is the Avogadro number, V represents the sample' droplet volume, C_{SERS} and C_{Raman} are the R6G molar concentration used in SERS and Raman measurements, respectively, A_{laser} is the laser spot area and A_{SERS} and A_{Raman} are the substrate area.

2.6. Proof-of-concept: SARS-CoV-2 spike protein screening

As a proof-of-concept, the optimized SERS membrane was used for SARS-CoV-2 spike protein screening by measuring its intrinsic spectra at two different concentrations: 2000 and 5 ng/ml. 2

µl of samples were deposited in the SERS membrane and the obtained spectra represented the average of three measurements.

3. Results and discussion

3.1. Solution-based gold nanoparticles synthesis

Initially, a study on the dependence of AuNPs properties from reactant's concentration and type of chemical reducing agent was conducted to select proper parameters for the in situ SERS membranes fabrication. $HAuCl_4$ was used as the precursor and tested at concentrations of 0.5 and 1.0 mM. As for RAs, the nanoparticles were synthesized with Na_3Ct, following a modified Turkevich method[44] and with glucose, at the concentrations of 2.5 and 5.0 mM. This was performed for 10 min at 120 ºC, assisted by microwave irradiation. In addition, when glucose was used as RA, the syntheses were also performed at RT, without microwave irradiation, since it is reported in the literature, glucose-based AuNPs production promoted by an alkaline medium at room temperature.[45–47] However, the synthesis outcome showed a poor reproducibility as optical properties is concerned, with variable surface plasmon resonance (SPR) and maximum absorbance values (Figure S1). For this reason, this approach was disregarded in further optimizations.

The optical properties and morphology of AuNPs produced using both Na_3Ct and glucose through microwave irradiation were assessed by UV-Vis spectroscopy and TEM, respectively (Figure 1).

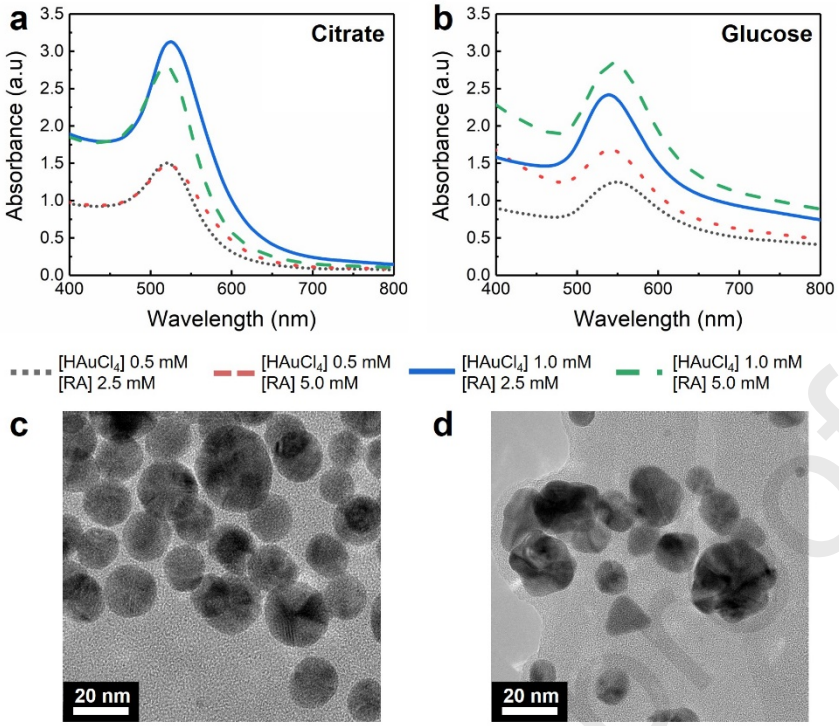

Figure 1 Optical properties of the synthesized gold nanoparticles at different concentrations of precursor and reducing agents. a: UV-Vis average spectra (n=3) of citrate-based gold nanoparticles; b: UV-Vis average spectra (n=3) of glucose-based gold nanoparticles; c: Representative TEM image of citrate-based gold nanoparticles; d: Representative TEM image of glucose-based gold nanoparticles.

As expected, a SPR band was observed for all the syntheses, thus confirming the successful growth of the AuNPs. Reproducibility was assessed by repeating each synthesis in triplicate and evaluating the resulting optical properties. In general, a good reproducibility was achieved for both citrate and glucose-based syntheses with microwave irradiation, evidenced by the calculated low standard deviations (Table S1).

The reaction for the synthesis of AuNPs by citrate and glucose reduction is based on the oxidation of the reducing agents to dicarboxy acetone and gluconic acid, respectively, with subsequent reduction of Au^{3+} to Au^{0}.[46,48] In both cases, the reducing agents act also as a capping agent, contributing to the formation of an outer shell of anionic charges (from the carboxylate groups in citrate) or hydroxyl groups (from glucose).[49,50]

For both syntheses, the absorbance values obtained rose when higher concentrations of gold salt precursor were used (Figure 1a,b), which may be indicative of an increased number of AuNPs, when $HAuCl_4$ was in a higher concentration. This observation can be correlated with Polte, J. et al. [51] growth mechanism, explaining that the number of AuNPs is defined in the second stage

and a higher concentration of gold salt precursor leads to a higher amount of nuclei particles. The authors showed that the conventional LaMer model is unable to predict the evolution of nanoparticle's size distribution, only describing the process of nucleation followed by a growth of the stable nuclei. They demonstrated experimentally that the AuNPs formation mechanisms follow four main steps: in a first step, due to the high reduction rate, a rapid formation of clusters of particles with 1-2 nm occurs; then, in a second step, the reduction rate decreases which leads to the coalescence of the freshly formed clusters, translating in a decrease in the number of particles, until stabilization. The number of particles remains then constant throughout the rest of the synthesis process, and their growth in size occurs during the following steps. In the third step, the AuNPs continue their growth through a diffusional process of the reduced gold atoms present in solution and an electrical double layer is created around the AuNPs. Lastly, in the final step, the growth rate increases leading to a rapid reduction of the remaining gold salt, the nanoparticles achieve their final size, and the appearance of a ruby/red color is indicative of reaction completion. Figure 2 shows the obtained SPR values and AuNPs' diameter obtained by DLS for the citrate and glucose-based AuNPs.

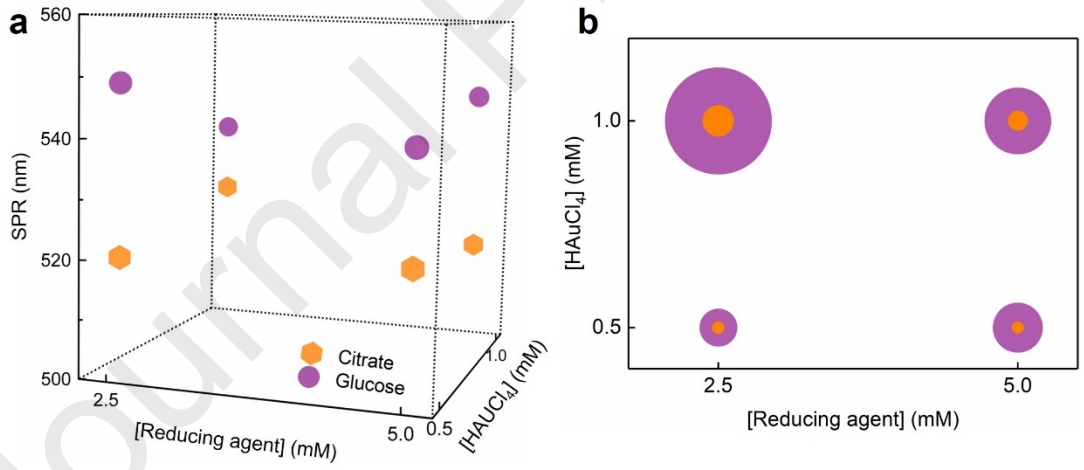

Figure 2 Analytical features calculated from the UV-Vis spectra of the synthesized AuNPs, by microwave irradiation, with citrate and glucose as reducing agents. a: SPR values as dependent of reactant's concentration; b: Bubble graph representation of AuNPs' diameter calculated by DLS. Absolute values for the present graph representation are presented in Table S1.

The obtained SPR values for citrate-based AuNPs, centered around 520 nm, and for glucose-based AuNPs, centered around 540 nm (Figure 2a), are in agreement with those reported in the literature.[49] Moreover, glucose-based AuNPs showed broader absorption bands than the citrate-based AuNPs, which can indicate a higher heterogeneity in size and/or shape of the

glucose-based AuNPs.[46] This was confirmed by TEM imaging (Figure 1c,d) where spherical particles are visible on the citrate-based AuNPs, whereas the AuNPs prepared with glucose shows anisotropic shapes.

As expected from the SPR values, citrate-based AuNPs have smaller particle' sizes than the glucose-based AuNPs (Figure 2b and Table S1). One possible explanation for the overall higher SPR and higher diameter of glucose-based AuNPs can be due to the possibility of hydrogen bonding of the hydroxyl groups present in the capping layer of these particles which leads to their agglutination. Moreover, a strong dependence of particles' diameter on the concentration of RA was observed, especially for citrate-based AuNPs: for constant $HAuCl_4$ concentrations, higher [RA] renders smaller AuNPs diameter, with higher influence in high $HAuCl_4$ concentrations. These results corroborate with literature data relating the quantity of reducing agent with the final particle size. A high amount of citrate ions strongly favors nucleation leading to a high quantity of nuclei which in turn results in smaller AuNPs, due to the rapid consumption of citrate for $HAuCl_4$ reduction.[51–54]

In the case of glucose, this correlation between RA concentration and final particle size was only observed for high concentrations of $HAuCl_4$. The SPR value and particle size can also be strongly influenced by the morphology and/or shape homogeneity of the NPs. In fact, these deviations are observed in the glucose-based AuNPs, since this reducing agent renders AuNPs with higher heterogeneity in terms of shape and size, as it was corroborated by TEM imaging (Figure 1d).[46]

The stability of the synthesized AuNPs was evaluated through visual inspection and direct comparison of the A_{SPR} value after 3 months of production (Figure 3).

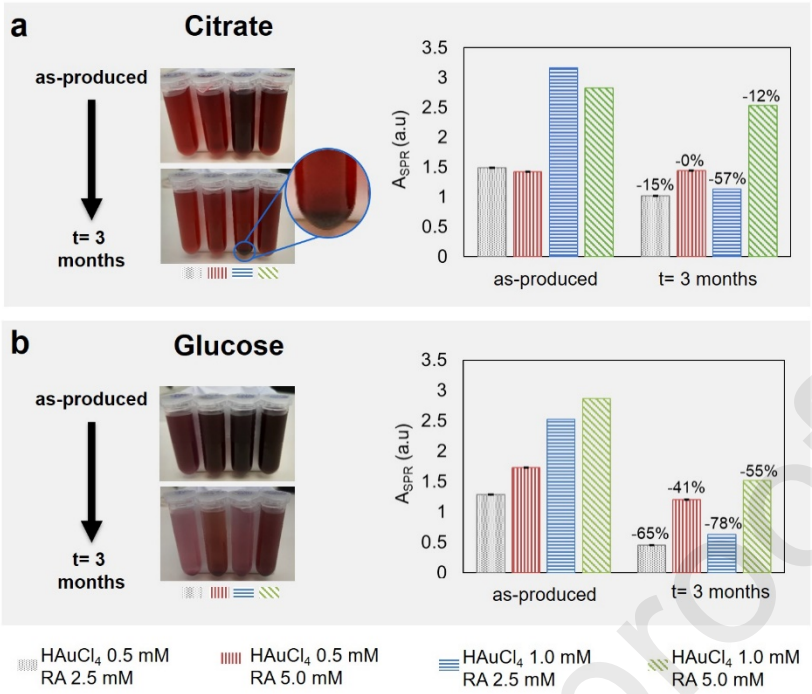

Figure 3 Stability evaluation of the synthesized AuNPs after 3 months of storage at 4 ºC. a: citrate-based AuNPs colloidal solutions photographs and calculated maximum absorbances; b: glucose-based AuNPs colloidal solutions photographs and calculated maximum absorbances. The percentage values represent the drop in the maximum absorbance value after 3 months of storage.

Exceptional high stability of the gold nanoparticles produced through citrate-based synthesis is observed, which shows the higher stability efficiency of citrate when compared to glucose.[50] After 3 months of storage at 4º C, the glucose-based AuNPs precipitated which translates in drops of the SPR absorbances from 41% to 78%. In fact, as mentioned above, this can be explained by the aglutination of glucose-based AuNPs through hydrogen bonding which leads to their precipitation. The highest drops are observed for 2.5 mM glucose which can indicate that this concentration is limitant, and it is not enough to efficiently stabilize the produced nanoparticles through a capping process. For the AuNPs produced through citrate reduction route, although lower than glucose-based nanoparticles, the highest decrease on A_{SPR} is also observed when 2.5 mM of reducing agent is used. In fact, a noticeable precipitate of AuNPs synthesized with 1.0 mM of $HAuCl_4$ and 2.5 mM of Na_3Ct is visible, which leads to a 57% reduction of the A_{SPR}. A possible explanation could be that when the reducing agent, which is responsible for both reduction and stabilization of the particles, is present in a low concentration, thus at a low reducing agent to gold ratio, it is not sufficient to efficiently cap the AuNPs, which leads to their aggregation,with consequent precipitation.[51]

For these reasons, Na_3Ct at 5.0 mM was chosen as the reducing agent and optimal concentration with 1.0 mM $HAuCl_4$ due to its highly stabilized AuNPs combined with a high maximum SPR absorbance, centered at 518 ± 2 nm, which is important to obtain a high loading of NPs onto cellulose-based SERS membranes, increasing the number of hot spots which leads to a more efficient Raman signal amplification.

3.2. SERS membranes fabrication: in situ synthesis of gold nanoparticles

The prepared NC membranes from *nata de coco* cubes were subjected to an in situ growth of AuNPs with the previously optimized conditions. Figure 4 shows the workflow to produce a NC membrane loaded with AuNPs.

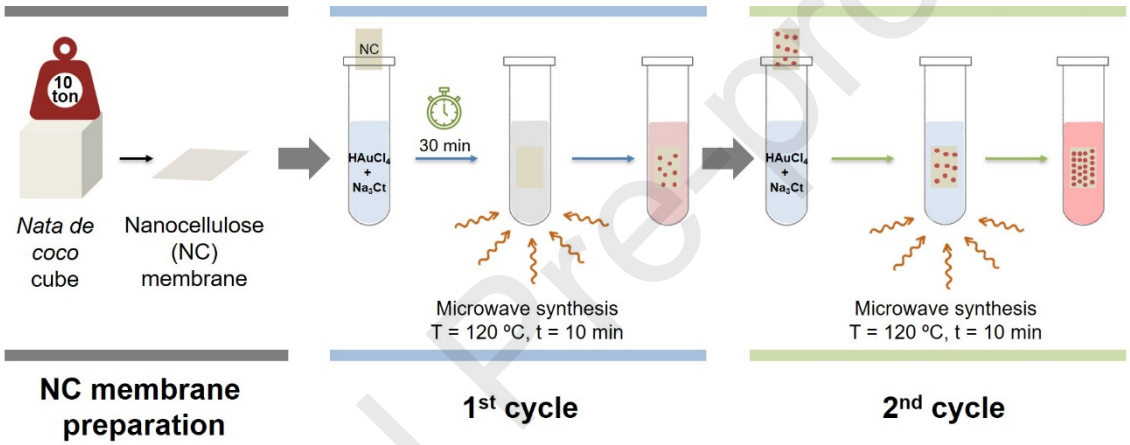

Figure 4 Schematic representation of AuNPs-based SERS membrane workflow production.

Briefly, a NC membrane was placed inside the microwave vessel, with the reaction mixture, and subjected to microwave irradiation for AuNPs synthesis. The as-prepared membrane was then transferred to a new microwave vessel with a freshly prepared reaction mixture and subjected again to microwave irradiation.

Figure 5 shows the resulting SEM images and optical photographs of the prepared NC@AuNPs membranes.

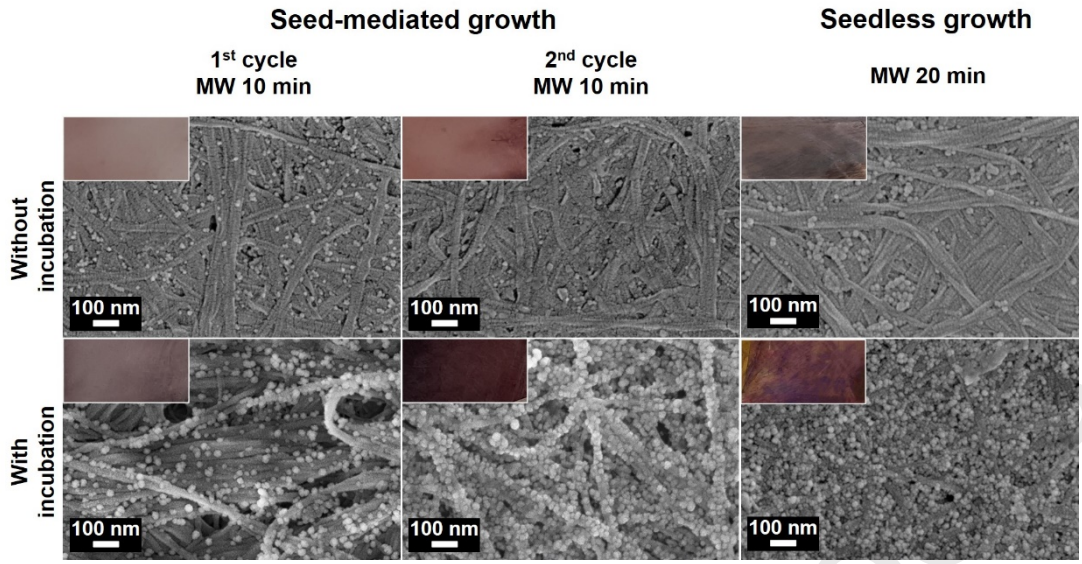

Figure 5 In situ synthesis of gold nanoparticles onto nanocellulose membranes via seed and seedless-mediated growth methods: SEM images and photographs of the resultant membranes. Direct comparison of the membranes with and without the 30 min incubation step.

The growth of the AuNPs onto the NC membrane was performed, in a first stage, by immersing the substrate in the reaction mixture and subjecting it immediately to microwave irradiation. The successful growth of AuNPs onto the NC fibers was confirmed by SEM imaging and by the light purple color of the obtained membrane. The as-prepared membrane was then used as a seed layer and subjected to a second cycle of synthesis (NC@AuNPs). An increase in the purple color intensity was observed, which may indicate the formation of larger clusters of AuNPs, as observed in the SEM image. However, these large clusters are heterogeneously dispersed throughout the NC fibers and at a very low density.

As it is known, the dispersion of closely-packed AuNPs throughout the substrate is critical for SERS performance, where the main contributor for high EF is the EM effect that can be magnified when the plasmonic NPs are close to each other, creating hot-spots.[17] To increase the AuNPs' density onto the NC membranes, an incubation time of 30 min preceded the seed-mediated growth process. We believe that this incubation time, prior to microwave irradiation, allowed the formation of pre-colloidal nuclei, visible by the change of the reaction mixture to a greyish color solution, and for an efficient nanocellulose' wicking of the reaction mixture. This led to an increase in the number of AuNPs loaded onto the NC membrane, compared to the same process without incubation (Figure 5). Additionally, the 2nd cycle of microwave synthesis revealed a full coverage of the NC fibers, visible in the SEM image and in the inset picture of NC_{inc}@AuNPs membrane that presents a dark purple color.

The XRD analysis performed on the SERS membranes obtained by the seed-mediated growth method, with and without the incubation step (NC_{inc}@AuNPs and NC@AuNPs, respectively), revealed the presence of the characteristic AuNPs crystallographic peaks (Figure 6a).

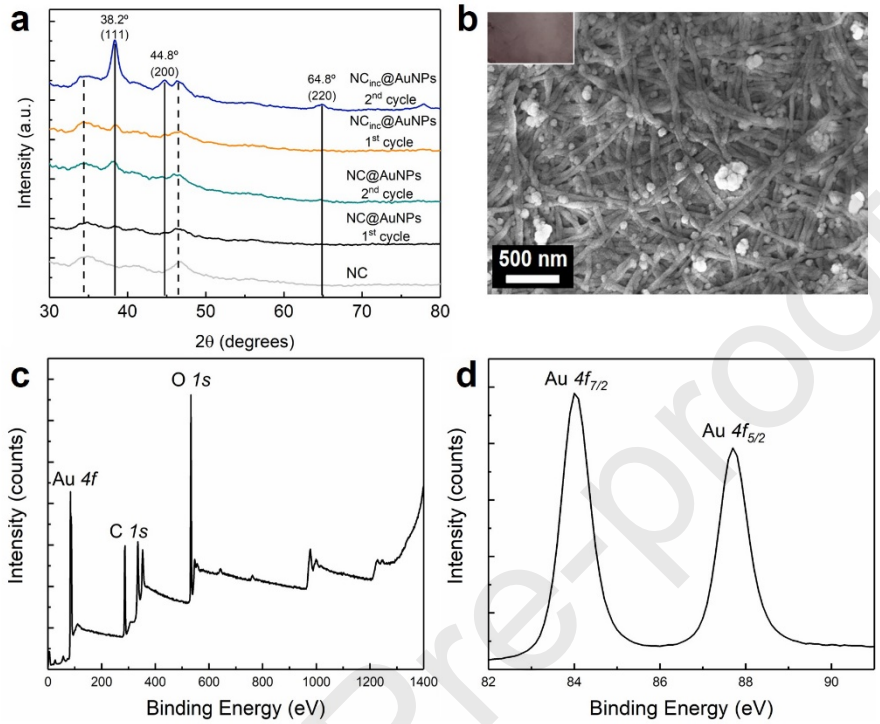

Figure 6 a. XRD diffractogram for the NC membrane with and without grown AuNPs on its fibers after each reaction cycle without and with the incubation step; b. SEM image and optical photograph of glucose-based NC membrane with grown AuNPs with the optimized conditions for citrate-based synthesis; c and d. XPS analysis of the optimized NC_{inc}@AuNPs SERS platform.

In addition, is it observed, especially in the most prominent peak at 38.2°, assigned to the (111) crystallographic plane,[55] an increase in its intensity from the 1st to the 2nd cycles, indicative of the increase in the AuNPs number. A XPS analysis was also performed to the final and optimized NC_{inc}@AuNPs membrane, with the incubation step and the seed-mediated growth method (Figure 6c,d). As expected, the presence of the peaks from oxygen (O *1s*) and carbon (C *1s*), from the capping layer, respectively centered at 533 and 287 eV, is visible (Figure 6c). The peak at 84 eV, assigned to Au $4f_{7/2}$, and the peak at 88 eV, attributed to Au $4f_{5/2}$, with a peak separation of 3.7 eV and with $I4f_{7/2} > I4f_{5/2}$ (Figure 6d), confirms the complete reduction of Au^{3+} to Au^0, reinforcing the successful growth of AuNPs.[56–59]

Having established the need for an incubation step, the necessity of a seed-mediated growth method instead of a seedless AuNPs growth onto the NC membrane was also investigated. For that, the reaction time was increased to 20 min, to assure that the homogeneous growth of AuNPs

was directly related to the seed and not to the total reaction time. These syntheses were performed by maintaining all the other microwave parameters and reactants concentration constant, without and with the incubation step. Although both cases lead to AuNPs' growth, confirmed by SEM and by the membranes' purple color, as expected, the synthesis carried out with the incubation step resulted in a NC membrane with a higher density of AuNPs. By directly comparing the SERS membranes obtained by the seed and seedless-mediated growth, with the incubation step (NC_{inc}@AuNPs and $NC_{inc\text{-}20min}$@AuNPs, respectively), it was possible to observe in both cases a good coverage of the NC fibers with the in situ synthesized AuNPs. However, a lower coverage of the cellulose fibers by the AuNPs is observed when compared with the seed-mediated growth method. This reveals the importance of having a seed for the subsequent growth of AuNPs and the importance of renew the reaction mixture offering more citrate and gold ions for the synthesis of more AuNPs.

Despite the better outcomes displayed by the solution-based citrate reduction route for the AuNPs synthesis, the previously optimized conditions for the preparation of SERS membranes (incubation step followed by a seed-mediated growth method) were mimicked using glucose as the RA. However, this synthesis method showed a poorer coverage of the cellulose' nanofibers and a very low AuNPs' density with bigger particles' sizes than the citrate-based synthesis, which is correlated with the results obtained in the solution-based synthesis (Figure 6b). A possible explanation for this was given by Xia and co-workers,[7] stating that the carbonyl groups of reducing agents can effectively absorb microwaves, facilitating the reduction process. In opposition to citrate that is composed of several carbonyl groups, glucose has five hydroxyl groups that compete for microwave absorption.

Additionally, the optimized in situ seed-mediated growth method for NC membranes was also performed with other cellulosic substrates: office paper, cardboard and Whatman paper grade 1. Due to the hydrophobic nature of both office paper and cardboard substrates, the synthesis rendered an inhomogeneous distribution of the AuNPs (Figure S2). On the contrary, the Whatman paper's hydrophilic nature allowed to successfully wick the reaction mixture, showing a homogeneous distribution and coverage of the AuNPs on the cellulose fibers (WP_{inc}@AuNPs) (Figure 7).

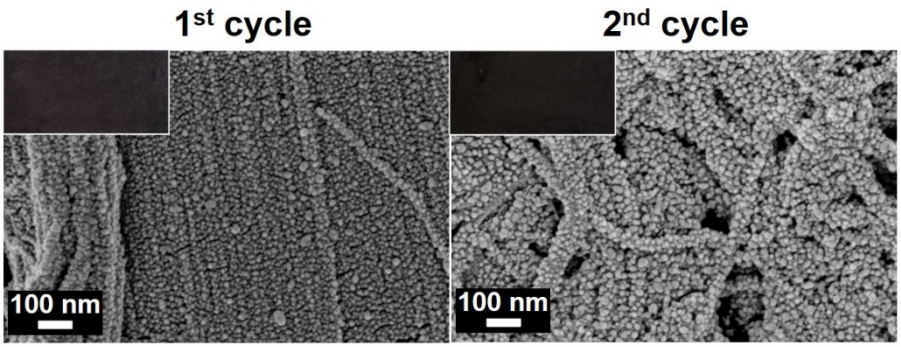

Figure 7 In situ synthesis of gold nanoparticles onto Whatman paper via a seed-mediated growth method, with a 30 min incubation step: SEM images and photographs of the resultant WP_{inc}@AuNPs.

Similarly to the NC membranes, an increase in the AuNPs density was visible from the 1st to 2nd cycle. However, comparing the outcome after 1st cycle of both substrates, the WP_{inc}@AuNPs seems to have a higher particle density. This feature can be due to a higher capillary action of Whatman paper and/or its higher grammage which can lead to the wicking of a superior amount of reaction mixture, resulting in a higher amount of in situ grown AuNPs. Nevertheless, an increase on the number of AuNPs after the 2nd reaction cycle was visible, with AuNPs fully covering the papers fibers, demonstrated by the SEM image and the darker color of the resulting WP_{inc}@AuNPs.

The average diameter size of the AuNPs obtained after each cycle was calculated for both NC and Whatman paper substrates, using the ImageJ software (Figure S3). Both substrates revealed AuNPs with similar sizes (27.6 ± 6 and 27.1 ± 7 nm for NC_{inc}@AuNPs and WP_{inc}@AuNPs, respectively), after the 2nd reaction cycle. However, after the 1st cycle, the NC_{inc}@AuNPs membrane had bigger particles (32.3 ± 8 nm) than the WP_{inc}@AuNPs membrane (17.8 ± 4 nm). This fact was explained by the faster wicking of the reaction mixture by the Whatman paper substrate, which can result in a faster AuNPs growth and consequently in nanoparticles with smaller sizes.

3.3. SERS performance evaluation

The ability of the prepared membranes to be used as SERS substrates was evaluated, using R6G as the probe molecule (Figure 8).

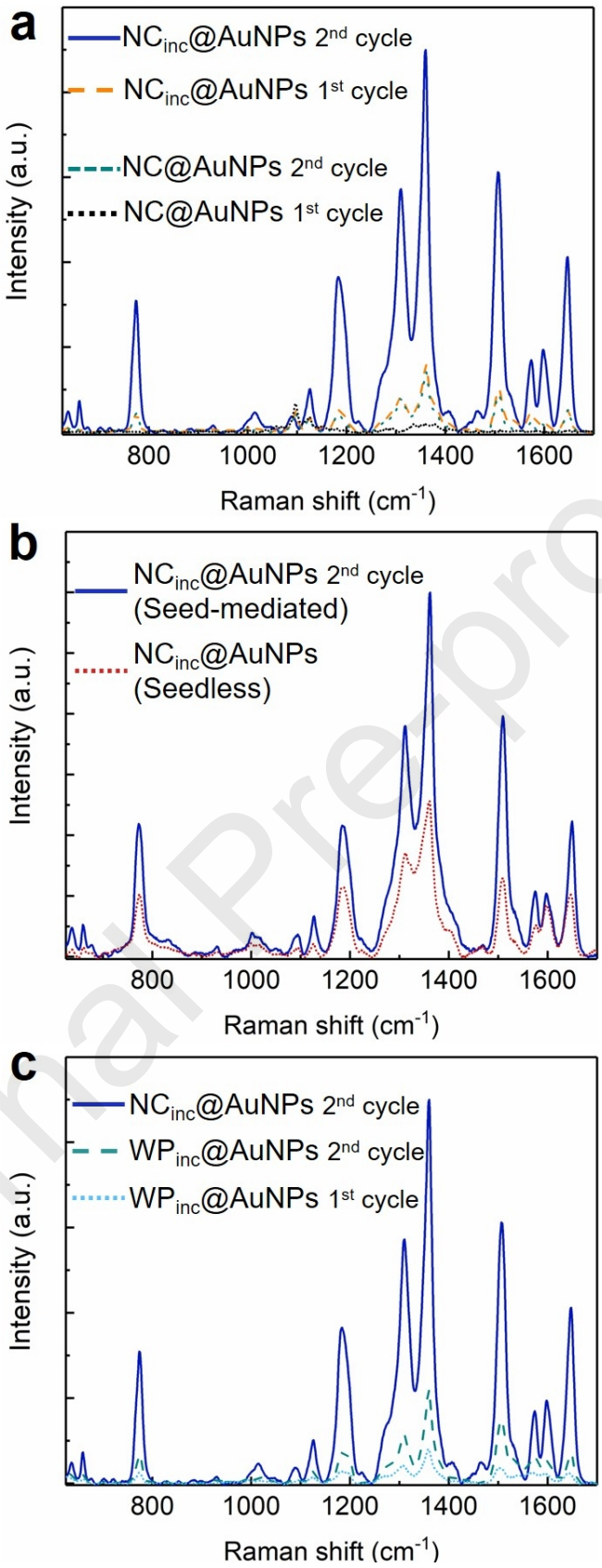

Figure 8 SERS performance evaluation of the prepared membranes: a. R6G SERS spectra obtained with SERS substrates after each reaction cycle, with and without the incubation step; b. R6G SERS spectra obtained with the SERS substrates by the seed and seedless-mediated growth methods; c. R6G SERS spectra obtained with the optimized SERS membranes with nanocellulose and Whatman paper substrate produced after each reaction cycle.

Figure 8a shows the R6G spectra obtained using the prepared NC@AuNPs and NC_{inc}@AuNPs membranes after the 1st and 2nd cycle of microwave irradiation. No R6G characteristic bands were observed with the NC@AuNPs membrane with one reaction cycle and without the incubation step. After the seed-mediated growth, it was possible to notice the R6G bands, although with low signal intensity. On the contrary, a high increase on R6G spectrum intensity was clearly visible, by 6-fold (using the intensity of the most intense band), for the NC_{inc}@AuNPs when compared with its counterpart NC@AuNPs, clearly showing the need and importance of the incubation step. In these cases, the main R6G characteristic bands were clearly present at 767 and 1184 cm^{-1} attributed to C-H out-of-plane bending and C-H in-plane bending vibrations, respectively. Additionally, the bands at 1360, 1508, 1570 and 1651 cm^{-1} were assigned to symmetric modes of in-plane C-C and C-O-C stretching vibrations.[17]

By comparing the membranes obtained with the incubation step followed by a seed-mediated and seedless growth (Figure 8b) it was evident that the membrane obtained by the seed-mediated growth had a better SERS performance. In fact, despite the NC_{inc}@AuNPs membranes obtained with the seedless growth showed well distributed AuNPs, with a good surface coverage, by comparing directly these membranes with the ones obtained through an optimized seed-mediated growth it was observed that the NPs had a higher surface coverage around the cellulose nanofibers in the second approach.

Finally, Figure 8c shows the comparison between the R6G SERS spectra of the optimized NC_{inc}@AuNPs membrane with the membranes produced using Whatman paper as substrate, after the 1st and 2nd cycle of synthesis. Regarding the WP_{inc}@AuNPs membranes, an increase in the SERS signal from the 1st to 2nd cycle of reaction is visible, due to a high amount of AuNPs distributed through the cellulose fibers. Additionally, a higher SERS intensity for the NC_{inc}@AuNPs membranes is observed. This can be explained by high surface area and surface-to-volume ratio of the NC substrate, and since SERS is a surface effect, it can benefit from having the analyte well dispersed in the surface of the SERS substrate. Despite the hydrophilic nature of both substrates and their three-dimensional morphology, which can lead to the absorption of the analyte throughout all the membranes' thickness, the NC substrate has a structure with low porous content and/or nanosized pores, which enables a higher availability of the analyte to the incident laser.

Additionally, the as-optimized SERS membranes were compared with a widely used immersion method to decorate supporting substrates with plasmonic nanostructures.[60–63] For that, an NC membrane was immersed in a AuNPs colloidal solution (prepared with optimized parameters, $HAuCl_4$ 1.0 mM with Na_3Ct 5.0 mM) for 24 h, allowed to dry at RT and the R6G spectra was recorded (Figure 9a).

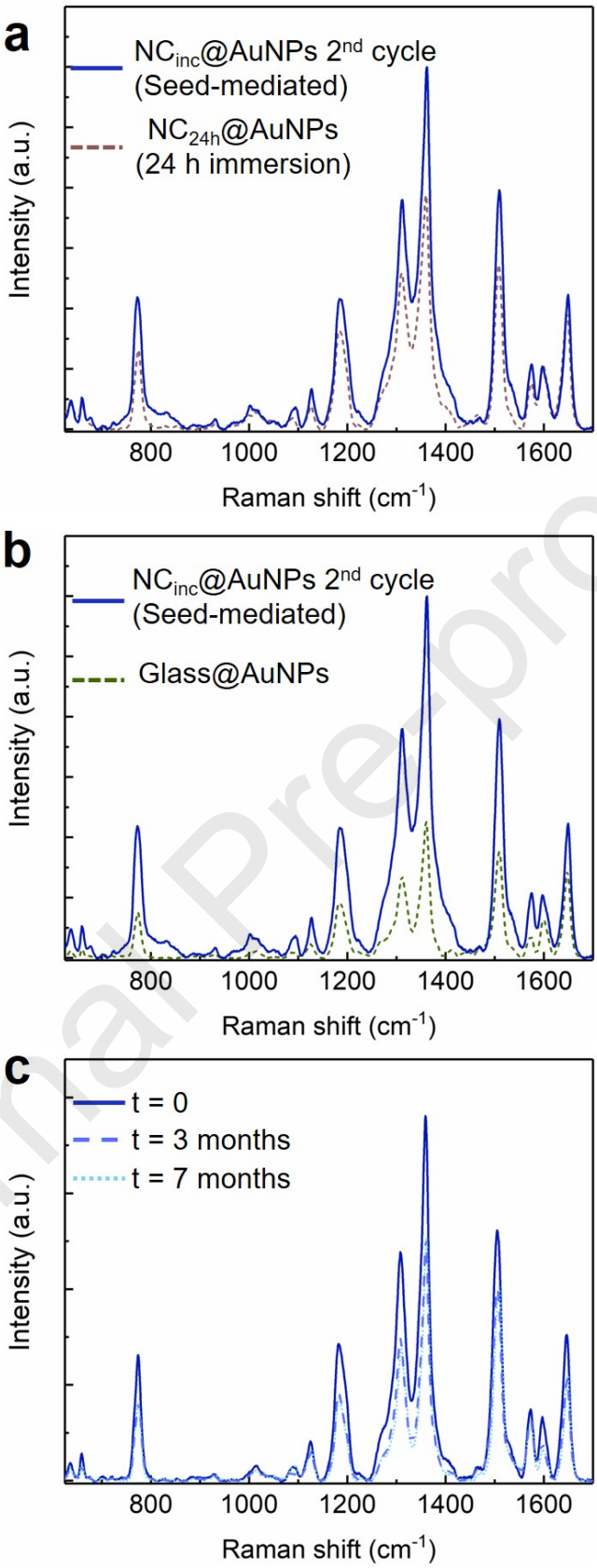

Figure 9 As-optimized SERS membrane performance: a. Comparison between R6G average SERS spectra (n=5) recorded on SERS membranes prepared with the optimized method and with a 24 h immersion method; b. Comparison between R6G average SERS spectra (n=5) recorded on SERS membranes prepared with the optimized method and on a glass substrate; b. R6G average SERS spectra (n = 5) obtained in the optimized NC$_{inc}$@AuNPs membrane after production, 3 and 7 months.

A direct comparison of the recorded R6G spectra on the NC_{inc}@AuNPs membranes with the ones prepared with the 24 hours immersion method reveals the enhanced performance of our approach, attaining overall higher SERS intensities with a much shorter preparation time. Moreover, to assess the importance of having a high surface area substrate for Raman signal amplification, a 2 µl volume of the AuNPs colloidal solution was deposited on a glass substrate and allowed to dry at RT. Figure 9b shows the obtained R6G spectra which reveals a lower SERS signal when compared with our substrate, evidencing the advantages of using cellulose-based substrates as supporting matrix for Raman enhancement nanostructures.

Within the most relevant figures of merit of SERS substrates are the EF, RSD, the cost, and the shelf life. The herein produced and optimized SERS platform achieved an EF up to ~10^6, with 10^{-6} M R6G, for both most intense peaks of 1360 and 1508 cm^{-1}, with an RSD lower than 8%, which confirm the best performance of our approach within the state of the art of AuNPs Raman enhancement.[64–66] In terms of cost, the use of a low-cost and commercially available substrate allied with a solution-based production method, with an energy-efficient synthesis method, reduces the final cost of the produced membranes significantly, within the cents range, well below the price of the substrates currently available in the market.

Finally, R6G SERS spectra were recorded over time to assess its shelf life (Figure 8c) showing a good performance even after 7 months of production. Accounting for the R6G more intense peak of 1360 cm^{-1} a 33% drop in its intensity was observed with the membrane after 3 months of production which remained stable after 7 months. Despite this intensity drop of R6G signal, its main characteristic peaks were still clearly identified, showing that the observed decrease did not have a significant impact upon SERS performance. This evidenced the long shelf life of the produced and optimized SERS membrane, even stored at room temperature without requiring special storage conditions.

1. Proof-of-concept: SARS-CoV-2 Spike protein detection

As a proof-of-concept, the as-prepared and optimized SERS membrane was used for screening the SARS-CoV-2 spike protein (S protein). The ongoing pandemic of coronavirus disease (COVID-19) caused by the severe acute respiratory syndrome coronavirus 2 (SARS-CoV-2) has caused to date (data accessed on 4th March, 2021)[67] more than 114 million cases and more

than 2.55 million deaths. Several diagnostic strategies and perspectives have been reported in the literature.[68,69] S protein was identified as one of the potential biomarkers to diagnose this disease.[70–72] A few works on SERS-based S protein screening have been reported in the literature. Zhang, D. et al has reported a SERS platform, based on sliver nanorods grown on a silicon substrate, for the recognition of S protein using the receptor angiotensin-converting enzyme 2 (ACE2) as biomarker.[73] Also, a work based on Ta_2C MXenes for Raman signal amplification was used for S protein recognition,[74] thus validated the SERS approach for COVID-19 diagnosis.

Herein, we show preliminary results for label-free S protein screening showing the feasibility of the developed SERS platform. (Figure 10).

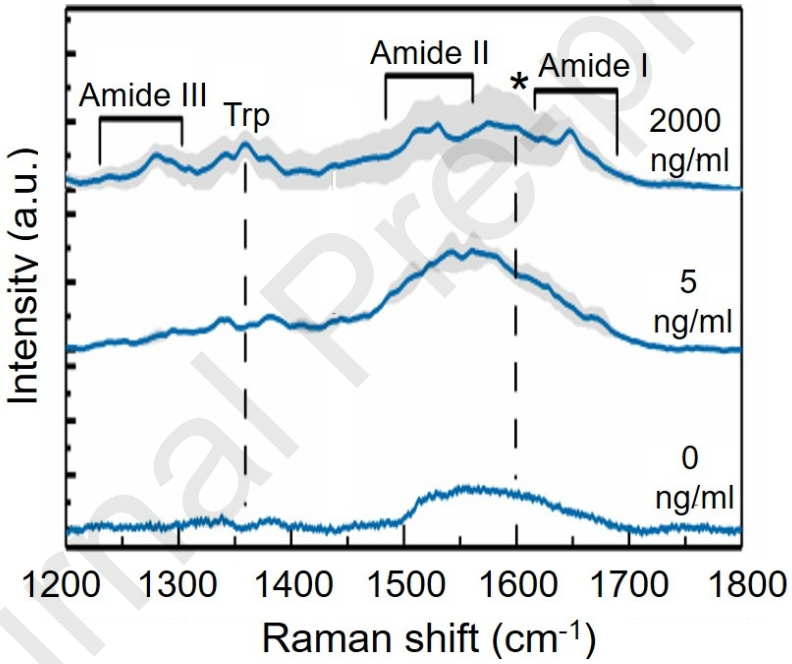

Figure 10 SERS spectra of S protein on the optimized SERS membranes. The grey area represents the average spectra (n=3).

The recorded average SERS spectra of S protein for 2000 and 5 ng/ml shows the characteristic bands of proteins. Amide I region is identified in 1600-1690 cm^{-1} associated with C=O stretching, Amide II in 1480-1575 cm^{-1} and Amide III in 1229-1301 cm^{-1} caused by CN stretching and NH bending. Additionally, the peak at 1361 cm^{-1} is attributed to Trp the zone marked with an * can be attributed to aminoacid Phenylalanine (Phe) or Tyrosine (Tyr) and Tryptophan (Trp) residues

bands.[75,76] We believe that these results can be seen as an initial evidence of label-free COVID-19 diagnosis through the use of a highly stable and low-cost platform.

4. Conclusions

In this work, a systematic study on fabrication of NC-based SERS platforms, prepared with a in situ microwave-assisted synthesis method was performed by optimizing relevant parameters. Citrate-based AuNPs has proven to provide enhanced optical properties and stability over time, when compared with glucose-based synthesis. Our fabrication approach based on an incubation step of the cellulosic substrate on the reaction mixture followed by seed-mediated growth method of AuNPs, rendered membranes with well-distributed and densely packed NPs. The method was employed in close-to-hydrophobic and hydrophilic cellulose substrates, with better outcomes obtained with hydrophilic ones due to the high capacity to wick the reaction mixture translating in a homogeneous distribution of particles. Moreover, in terms of SERS performance, NC had superior results when compared to Whatman paper due to its less porous structure and high surface area. A calculated EF of around 10^6 was attained, with an RSD lower than 8% and an outstanding shelf life up to 7 months, with regular storage conditions, for the herein optimized NC_{inc}@AuNPs SERS platform. Our developed workflow for SERS membranes fabrication translates in higher Raman amplifications than a 24 h immersion method, with obvious benefits in terms of reduction of total fabrication time. Additionally, the benefits of using a three-dimensional material with high surface-to-volume ratio as SERS supporting matrix was demonstrated with the enhanced SERS intensities obtained with our membrane, when compared to a common glass substrate decorated with AuNPs.

We believe that the herein developed SERS membrane offers an accurate, reliable and inexpensive platform for biosensing that can be used in point-of-care settings when combined with a portable Raman reader.

Acknowledgements

This work is funded by National Funds through FCT I.P., under the scope of the project UIDB/50025/2020-2023. The authors acknowledge the ERC AdG project DIGISMART ref. 787410 and EC project SYNERGY H2020-WIDESPREAD-2020-5, CSA, proposal nº 952169. Also, the authors thank funding co-financed by the Operational Programme for Competitiveness

and Internationalisation (COMPETE 2020) and Lisbon Regional Operational Programme (Lisboa 2020), under the PORTUGAL 2020 Partnership Agreement, through the European Regional Development Fund (ERDF) under the projects ECO2COVID ref. 68174 and TecniCOV ref. 69745. A. C. Marques acknowledges funding from FCT I.P., through the PhD Grant SFRH/BD/115173/2016. The authors acknowledge Professor Pedro Costa from KAUST for the TEM imaging.

Additional information

Supplementary information: Supplementary information of this work is supplied free of charge.

Competing financial interests: The authors declare no competing financial interests.

References

[1] J. Jiang, Q. Shen, P. Xue, H. Qi, Y. Wu, Y. Teng, Y. Zhang, Y. Liu, X. Zhao, X. Liu, A Highly Sensitive and Stable SERS Sensor for Malachite Green Detection Based on Ag Nanoparticles In Situ Generated on 3D MoS2 Nanoflowers, ChemistrySelect. 5 (2020) 354–359. https://doi.org/10.1002/slct.201903924.

[2] K.C. Hsu, D.H. Chen, Microwave-assisted green synthesis of Ag/reduced graphene oxide nanocomposite as a surface-enhanced Raman scattering substrate with high uniformity, Nanoscale Res. Lett. 9 (2014) 1–9. https://doi.org/10.1186/1556-276X-9-193.

[3] K.A. Willets, R.P. Van Duyne, Localized Surface Plasmon Resonance Spectroscopy and Sensing, Annu. Rev. Phys. Chem. 58 (2007) 267–297. https://doi.org/10.1146/annurev.physchem.58.032806.104607.

[4] Principles of Surface-Enhanced Raman Spectroscopy, Elsevier, 2009. https://doi.org/10.1016/B978-0-444-52779-0.X0001-3.

[5] J.R. Lombardi, R.L. Birke, A Unified View of Surface-Enhanced Raman Scattering, Acc. Chem. Res. 42 (2009) 734–742. https://doi.org/10.1021/ar800249y.

[6] C. Lux, A. Lubio, A. Ruediger, S. Robert, C. Muehlethaler, Optimizing the analysis of dyes by Surface-Enhanced Raman Spectroscopy (SERS) using a conventional-microwave silver nanoparticles synthesis, Forensic Chem. 16 (2019). https://doi.org/10.1016/j.forc.2019.100186.

[7] L. Xia, H. Wang, J. Wang, K. Gong, Y. Jia, H. Zhang, M. Sun, Microwave-assisted synthesis of sensitive silver substrate for surface-enhanced Raman scattering spectroscopy, J. Chem. Phys. 129 (2008) 1–8. https://doi.org/10.1063/1.2987705.

[8] A.C. Marques, L. Santos, M.N. Costa, J.M. Dantas, P. Duarte, A. Gonçalves, R. Martins, C.A. Salgueiro, E. Fortunato, Office Paper Platform for Bioelectrochromic Detection of Electrochemically Active Bacteria using Tungsten Trioxide Nanoprobes, Sci. Rep. 5 (2015) 9910. https://doi.org/10.1038/srep09910.

[9] A. Pimentel, S.H. Ferreira, D. Nunes, T. Calmeiro, R. Martins, E. Fortunato, Microwave Synthesized ZnO Nanorod Arrays for UV Sensors: A Seed Layer Annealing Temperature Study, Materials (Basel). 9 (2016) 299. https://doi.org/10.3390/ma9040299.

[10] T. Jiang, J. Li, L. Zhang, B. Wang, J. Zhou, Microwave assisted in situ synthesis of Ag-NaCMC films and their reproducible surface-enhanced Raman scattering signals, J. Alloys Compd. 602 (2014) 94–100. https://doi.org/10.1016/j.jallcom.2014.03.020.

[11] A. Pimentel, A. Araújo, B.J. Coelho, D. Nunes, M.J. Oliveira, M.J. Mendes, H. Águas, R. Martins, E. Fortunato, 3D ZnO/Ag surface-enhanced Raman scattering on disposable and flexible cardboard platforms, Materials (Basel). 10 (2017). https://doi.org/10.3390/ma10121351.

[12] S. Dong, Y. Wang, Z. Liu, W. Zhang, K. Yi, X. Zhang, X. Zhang, C. Jiang, S. Yang, F. Wang, X. Xiao, Beehive-Inspired Macroporous SERS Probe for Cancer Detection through Capturing and Analyzing Exosomes in Plasma, ACS Appl. Mater. Interfaces. 12 (2020) 5136–5146. https://doi.org/10.1021/acsami.9b21333.

[13] N. Ferreira, A. Marques, H. Águas, H. Bandarenka, R. Martins, C. Bodo, B. Costa-Silva, E. Fortunato, Label-Free Nanosensing Platform for Breast Cancer Exosome Profiling, ACS Sensors. 4 (2019) 2073–2083. https://doi.org/10.1021/acssensors.9b00760.

[14] W. Kim, J.C. Lee, G.J. Lee, H.K. Park, A. Lee, S. Choi, Low-Cost Label-Free Biosensing Bimetallic Cellulose Strip with SILAR-Synthesized Silver Core-Gold Shell Nanoparticle Structures, Anal. Chem. 89 (2017) 6448–6454. https://doi.org/10.1021/acs.analchem.7b00300.

[15] S. Su, C. Zhang, L. Yuwen, J. Chao, X. Zuo, X. Liu, C. Song, C. Fan, L. Wang, Creating SERS hot spots on MoS2 nanosheets with in situ grown gold nanoparticles, ACS Appl. Mater. Interfaces. 6 (2014) 18735–18741. https://doi.org/10.1021/am5043092.

[16] R. Reid, B. Chatterjee, S.J. Das, S. Ghosh, T.K. Sharma, Application of aptamers as molecular recognition elements in lateral flow assays, Anal. Biochem. 593 (2020) 113574. https://doi.org/10.1016/j.ab.2020.113574.

[17] H. Li, X. Yue, N. Gao, J. Tang, X. Lv, J. Hou, Microwave method synthesis of magnetic ionic liquid/gold nanoparticles as ultrasensitive SERS substrates for trace clopidol detection, Anal. Bioanal. Chem. 412 (2020) 3063–3071. https://doi.org/10.1007/s00216-020-02588-7.

[18] X. Chen, J. Wen, J. Zhou, Z. Zheng, D. An, H. Wang, W. Xie, R. Zhan, N. Xu, J. Chen, J. She, H. Chen, S. Deng, Superhydrophobic SERS substrates based on silicon hierarchical nanostructures, J. Opt. 20 (2018) 024012. https://doi.org/10.1088/2040-8986/aaa100.

[19] K. Nemciauskas, L. Traksele, A. Salaseviciene, V. Snitka, A silicon membrane-silver nanoparticles SERS chip for trace molecules detection, Microelectron. Eng. 225 (2020) 111282. https://doi.org/10.1016/j.mee.2020.111282.

[20] X. Yue, X. Zheng, G. Lv, J. Mo, X. Yu, J. Liu, Z. Jia, X. Lv, J. Tang, Synthesis of a low-cost, stable, silicon-based SERS substrate for rapid, nondestructive biosensing, Optik (Stuttg). 192 (2019) 162959. https://doi.org/10.1016/j.ijleo.2019.162959.

[21] G. Yin, S. Bai, X. Tu, Z. Li, Y. Zhang, W. Wang, J. Lu, D. He, Highly Sensitive and Stable SERS Substrate Fabricated by Co-sputtering and Atomic Layer Deposition, Nanoscale Res. Lett. 14 (2019) 168. https://doi.org/10.1186/s11671-019-2997-8.

[22] C.C. Huang, C.Y. Cheng, Y.S. Lai, Paper-based flexible surface enhanced Raman scattering platforms and their applications to food safety, Trends Food Sci. Technol. 100 (2020) 349–358. https://doi.org/10.1016/j.tifs.2020.04.019.

[23] A. Araújo, A. Pimentel, M.J. Oliveira, M.J. Mendes, R. Franco, E. Fortunato, H. Águas, R. Martins, Direct growth of plasmonic nanorod forests on paper substrates for low-cost flexible 3D SERS platforms, Flex. Print. Electron. 2 (2017). https://doi.org/10.1088/2058-8585/2/1/014001.

[24] L. Chen, B. Ying, P. Song, X. Liu, A Nanocellulose-Paper-Based SERS Multiwell Plate with High Sensitivity and High Signal Homogeneity, Adv. Mater. Interfaces. 6 (2019). https://doi.org/10.1002/admi.201901346.

[25] M.J. Oliveira, P. Quaresma, M.P. De Almeida, A. Araújo, E. Pereira, E. Fortunato, R. Martins, R. Franco, H. Águas, Office paper decorated with silver nanostars-an alternative cost effective platform for trace analyte detection by SERS, Sci. Rep. 7 (2017). https://doi.org/10.1038/s41598-017-02484-8.

[26] A.T. Vicente, A. Araújo, D. Gaspar, L. Santos, A.C. Marques, M.J. Mendes, L. Pereira, E. Fortunato, R. Martins, Optoelectronics and Bio Devices on Paper Powered by Solar Cells, in: Nanostructured Sol. Cells, InTech, 2017: pp. 33–65. https://doi.org/10.5772/66695.

[27] H. Chen, M.B. Mbanjwa, T. Joubert, Paper-based smart microfluidics for education and low-cost diagnostics, 111 (2015) 1–10.

[28] A.W.A. Martinez, S.T.S. Phillips, G.M.G. Whitesides, E. Carrilho, Diagnostics for the Developing World: Microfluidic Paper-Based Analytical Devices, Anal. Chem. 82 (2010) 3–10. https://doi.org/10.1021/ac9013989.

[29] A. Parnsubsakul, U. Ngoensawat, T. Wutikhun, T. Sukmanee, C. Sapcharoenkun, P. Pienpinijtham, S. Ekgasit, Silver nanoparticle/bacterial nanocellulose paper composites for paste-and-read SERS detection of pesticides on fruit surfaces, Carbohydr. Polym. 235 (2020). https://doi.org/10.1016/j.carbpol.2020.115956.

[30] E. Fortunato, D. Gaspar, P. Duarte, L. Pereira, H. Águas, A. Vicente, F. Dourado, M. Gama, R. Martins, Optoelectronic Devices from Bacterial NanoCellulose, in: Bact. Nanocellulose, Elsevier, 2016: pp. 179–197. https://doi.org/10.1016/B978-0-444-63458-0.00011-1.

[31] T. VoDinh, M.Y.K. Hiromoto, G.M. Begun, R.L. Moody, Surface-Enhanced Raman Spectrometry for Trace Organic Analysis, Anal. Chem. 56 (1984) 1667–1670. https://doi.org/10.1021/ac00273a029.

[32] C.D. Tran, Subnanogram Detection of Dyes on Filter Paper by Surface-Enhanced Raman Scattering Spectrometry, Anal. Chem. 56 (1984) 824–826. https://doi.org/10.1021/ac00268a057.

[33] Z. Xiong, X. Chen, P. Liou, M. Lin, Development of nanofibrillated cellulose coated with gold nanoparticles for measurement of melamine by SERS, Cellulose. 24 (2017) 2801–2811. https://doi.org/10.1007/s10570-017-1297-7.

[34] G. Kwon, J. Kim, D. Kim, Y. Ko, Y. Yamauchi, J. You, Nanoporous cellulose paper-based SERS platform for multiplex detection of hazardous pesticides, Cellulose. 26 (2019) 4935–4944. https://doi.org/10.1007/s10570-019-02427-8.

[35] A. Marques, B. Veigas, A. Araújo, B. Pagará, P.V. Baptista, H. Águas, R. Martins, E. Fortunato, Paper-Based SERS Platform for One-Step Screening of Tetracycline in Milk, Sci. Rep. 9 (2019) 17922. https://doi.org/10.1038/s41598-019-54380-y.

[36] M. Chen, Z. Zhang, M. Liu, C. Qiu, H. Yang, X. Chen, In situ fabrication of label-free optical sensing paper strips for the rapid surface-enhanced Raman scattering (SERS) detection of brassinosteroids in plant tissues, Talanta. 165 (2017) 313–320. https://doi.org/10.1016/j.talanta.2016.12.072.

[37] W. Luo, M. Chen, N. Hao, X. Huang, X. Zhao, Y. Zhu, H. Yang, X. Chen, In situ synthesis of gold nanoparticles on pseudo-paper films as flexible SERS substrate for sensitive detection of surface organic residues, Talanta. 197 (2019) 225–233. https://doi.org/10.1016/j.talanta.2018.12.099.

[38] R.J.B. Pinto, P.A.A.P. Marques, A.M. Barros-Timmons, T. Trindade, C.P. Neto, Novel SiO2/cellulose nanocomposites obtained by in situ synthesis and via polyelectrolytes assembly, Compos. Sci. Technol. 68 (2008) 1088–1093. https://doi.org/10.1016/j.compscitech.2007.03.001.

[39] L. Kang, Y. Gao, H. Luo, Z. Chen, J. Du, Z. Zhang, Nanoporous thermochromic VO2 films with low optical constants, enhanced luminous transmittance and thermochromic properties, ACS Appl. Mater. Interfaces. 3 (2011) 135–138. https://doi.org/10.1021/am1011172.

[40] D. Deng, Q. Lin, H. Li, Z. Huang, Y. Kuang, H. Chen, J. Kong, Rapid detection of malachite green residues in fish using a surface-enhanced Raman scattering-active glass fiber paper prepared by in situ reduction method, Talanta. 200 (2019) 272–278. https://doi.org/10.1016/j.talanta.2019.03.021.

[41] M. Wu, P. Li, Q. Zhu, M. Wu, H. Li, F. Lu, Functional paper-based SERS substrate for rapid and sensitive detection of Sudan dyes in herbal medicine, Spectrochim. Acta - Part A Mol. Biomol. Spectrosc. 196 (2018) 110–116. https://doi.org/10.1016/j.saa.2018.02.014.

[42] S. He, J. Chua, E.K.M. Tan, J.C.Y. Kah, Optimizing the SERS enhancement of a facile gold nanostar immobilized paper-based SERS substrate, RSC Adv. 7 (2017) 16264–16272. https://doi.org/10.1039/c6ra28450g.

[43] M.J. Oliveira, P. Quaresma, M. Peixoto de Almeida, A. Araújo, E. Pereira, E. Fortunato, R. Martins, R. Franco, H. Águas, Office paper decorated with silver nanostars - an alternative cost effective platform for trace analyte detection by SERS, Sci. Rep. 7 (2017) 2480. https://doi.org/10.1038/s41598-017-02484-8.

[44] J. Turkevich, P.C. Stevenson, J. Hillier, A study of the nucleation and growth processes in the synthesis of colloidal gold, Discuss. Faraday Soc. 11 (1951) 55–75. https://doi.org/10.1039/DF9511100055.

[45] S. Unser, I. Campbell, D. Jana, L. Sagle, Direct glucose sensing in the physiological range through plasmonic nanoparticle formation, Analyst. 140 (2015) 590–599. https://doi.org/10.1039/C4AN01496K.

[46] T. Pinheiro, J. Ferrão, A.C. Marques, M.J. Oliveira, N.M. Batra, P.M.F.J. Costa, M.P. Macedo, H. Águas, R. Martins, E. Fortunato, Paper-Based In-Situ Gold Nanoparticle Synthesis for Colorimetric, Non-Enzymatic Glucose Level Determination, Nanomaterials. 10 (2020) 2027. https://doi.org/10.3390/nano10102027.

[47] T. Pinheiro, A.C. Marques, P. Carvalho, R. Martins, E. Fortunato, Paper Microfluidics and Tailored Gold Nanoparticles for Nonenzymatic, Colorimetric Multiplex Biomarker Detection, ACS Appl. Mater. Interfaces. 13 (2021) 3576–3590. https://doi.org/10.1021/acsami.0c19089.

[48] M. Tran, R. DePenning, M. Turner, S. Padalkar, Effect of citrate ratio and temperature on gold nanoparticle size and morphology, Mater. Res. Express. 3 (2016) 105027. https://doi.org/10.1088/2053-1591/3/10/105027.

[49] S. Suvarna, U. Das, K.C. Sunil, S. Mishra, M. Sudarshan, K. Das Saha, S. Dey, A. Chakraborty, Y. Narayana, Synthesis of a novel glucose capped gold nanoparticle as a better theranostic candidate, PLoS One. 12 (2017) 1–15. https://doi.org/10.1371/journal.pone.0178202.

[50] J.-W. Park, J.S. Shumaker-Parry, Structural Study of Citrate Layers on Gold Nanoparticles: Role of Intermolecular Interactions in Stabilizing Nanoparticles, J. Am. Chem. Soc. 136 (2014) 1907–1921. https://doi.org/10.1021/ja4097384.

[51] J. Polte, Fundamental growth principles of colloidal metal nanoparticles - a new perspective, CrystEngComm. 17 (2015) 6809–6830. https://doi.org/10.1039/c5ce01014d.

[52] M.K. Bayazit, J. Yue, E. Cao, A. Gavriilidis, J. Tang, Controllable Synthesis of Gold Nanoparticles in Aqueous Solution by Microwave Assisted Flow Chemistry, ACS Sustain. Chem. Eng. 4 (2016) 6435–6442. https://doi.org/10.1021/acssuschemeng.6b01149.

[53] S.K. Seol, D. Kim, S. Jung, Y. Hwu, Microwave synthesis of gold nanoparticles: Effect of applied microwave power and solution pH, Mater. Chem. Phys. 131 (2011) 331–335. https://doi.org/10.1016/j.matchemphys.2011.09.050.

[54] S. Kumar, K.S. Gandhi, R. Kumar, Modeling of formation of gold nanoparticles by citrate method, Ind. Eng. Chem. Res. 46 (2007) 3128–3136. https://doi.org/10.1021/ie060672j.

[55] B. Ankamwar, Gold and silver nanoparticles used for SERS detection of S. aureus and E. coli , Nano Express. 1 (2020) 010020. https://doi.org/10.1088/2632-959x/ab85b4.

[56] E. Rodríguez-León, B.E. Rodríguez-Vázquez, A. Martínez-Higuera, C. Rodríguez-Beas, E. Larios-Rodríguez, R.E. Navarro, R. López-Esparza, R.A. Iñiguez-Palomares, Synthesis of Gold Nanoparticles Using Mimosa tenuiflora Extract, Assessments of Cytotoxicity, Cellular Uptake, and Catalysis, Nanoscale Res. Lett. 14 (2019) 334.

https://doi.org/10.1186/s11671-019-3158-9.

[57] E. Alegria, A. Ribeiro, M. Mendes, A. Ferraria, A. do Rego, A. Pombeiro, Effect of Phenolic Compounds on the Synthesis of Gold Nanoparticles and its Catalytic Activity in the Reduction of Nitro Compounds, Nanomaterials. 8 (2018) 320. https://doi.org/10.3390/nano8050320.

[58] M.P. Casaletto, A. Longo, A. Martorana, A. Prestianni, A.M. Venezia, XPS study of supported gold catalysts: the role of Au0 and Au+δ species as active sites, Surf. Interface Anal. 38 (2006) 215–218. https://doi.org/10.1002/sia.2180.

[59] J. Moulder, W. Stickle, P. Sobol, K. Bomben, Handbook of X-ray Photoelectron Spectroscopy, Perkin-Elmer Corporation, 1992.

[60] J.E.L. Villa, N.R. Quiñones, F. Fantinatti-Garboggini, R.J. Poppi, Fast discrimination of bacteria using a filter paper–based SERS platform and PLS-DA with uncertainty estimation, Anal. Bioanal. Chem. 411 (2019) 705–713. https://doi.org/10.1007/s00216-018-1485-9.

[61] S. Dalla Marta, C. Novara, F. Giorgis, A. Bonifacio, V. Sergo, Optimization and characterization of paper-made Surface Enhanced Raman Scattering (SERS) substrates with Au and Ag NPs for quantitative analysis, Materials (Basel). 10 (2017). https://doi.org/10.3390/ma10121365.

[62] C.H. Lee, L. Tian, S. Singamaneni, Paper-based SERS swab for rapid trace detection on real-world surfaces, ACS Appl. Mater. Interfaces. 2 (2010) 3429–3435. https://doi.org/10.1021/am1009875.

[63] Y.H. Ngo, D. Li, G.P. Simon, G. Garnier, Gold nanoparticle-paper as a three-dimensional surface enhanced raman scattering substrate, Langmuir. 28 (2012) 8782–8790. https://doi.org/10.1021/la3012734.

[64] N. V. Godoy, D. García-Lojo, F.A. Sigoli, J. Pérez-Juste, I. Pastoriza-Santos, I.O. Mazali, Ultrasensitive inkjet-printed based SERS sensor combining a high-performance gold nanosphere ink and hydrophobic paper, Sensors Actuators, B Chem. 320 (2020). https://doi.org/10.1016/j.snb.2020.128412.

[65] W. Luo, M. Chen, N. Hao, X. Huang, X. Zhao, Y. Zhu, H. Yang, In situ synthesis of gold nanoparticles on pseudo-paper films as flexible SERS substrate for sensitive detection of surface organic residues, Talanta. 197 (2019) 225–233. https://doi.org/10.1016/j.talanta.2018.12.099.

[66] W.A. Ameku, W.R. De Araujo, C.J. Rangel, R.A. Ando, T.R.L.C. Paixão, Gold Nanoparticle Paper-Based Dual-Detection Device for Forensics Applications, ACS Appl. Nano Mater. 2 (2019) 5460–5468. https://doi.org/10.1021/acsanm.9b01057.

[67] World Health Organization, WHO Coronavirus Disease (COVID-19) Dashboard, (n.d.). https://covid19.who.int/ (accessed February 10, 2021).

[68] G. Mahesh, Paper-based Diagnostics for COVID-19 Developed by CSIR-IGIB, Sicence Report. (2020) 28–29.

[69] B. Udugama, P. Kadhiresan, H.N. Kozlowski, A. Malekjahani, M. Osborne, V.Y.C. Li, H. Chen, S. Mubareka, J.B. Gubbay, W.C.W. Chan, Diagnosing COVID-19: The Disease and Tools for Detection, ACS Nano. 14 (2020) 3822–3835. https://doi.org/10.1021/acsnano.0c02624.

[70] A.N. Baker, S.J. Richards, C.S. Guy, T.R. Congdon, M. Hasan, A.J. Zwetsloot, A. Gallo, J.R. Lewandowski, P.J. Stansfeld, A. Straube, M. Walker, S. Chessa, G. Pergolizzi, S. Dedola, R.A. Field, M.I. Gibson, The SARS-COV-2 Spike Protein Binds Sialic Acids and Enables Rapid Detection in a Lateral Flow Point of Care Diagnostic Device, ACS Cent. Sci. 6 (2020) 2046–2052. https://doi.org/10.1021/acscentsci.0c00855.

[71] D.R. Hristov, H. Rijal, J. Gomez-Marquez, K. Hamad-Schifferli, Developing a paper-based antigen assay to differentiate between coronaviruses and SARS-CoV-2 Spike variants,

ChemRxiv. (2020). https://doi.org/10.26434/chemrxiv.13476738.v1.

[72] X. Ou, Y. Liu, X. Lei, P. Li, D. Mi, L. Ren, L. Guo, R. Guo, T. Chen, J. Hu, Z. Xiang, Z. Mu, X. Chen, J. Chen, K. Hu, Q. Jin, J. Wang, Z. Qian, Characterization of spike glycoprotein of SARS-CoV-2 on virus entry and its immune cross-reactivity with SARS-CoV, Nat. Commun. 11 (2020). https://doi.org/10.1038/s41467-020-15562-9.

[73] D. Zhang, X. Zhang, R. Ma, S. Deng, X. Wang, X. Zhang, X. Huang, Y. Liu, G. Li, J. Qu, Y. Zhu, J. Li, Ultra-fast and onsite interrogation of severe acute respiratory syndrome coronavirus 2 (SARS-CoV-2) in environmental specimens via surface enhanced Raman scattering (SERS), MedRxiv. (2020). https://doi.org/10.1101/2020.05.02.20086876.

[74] Y. Peng, C. Lin, L. Long, T. Masaki, M. Tang, L. Yang, J. Liu, Z. Huang, Z. Li, X. Luo, J.R. Lombardi, Y. Yang, Charge-Transfer Resonance and Electromagnetic Enhancement Synergistically Enabling MXenes with Excellent SERS Sensitivity for SARS-CoV-2 S Protein Detection, Nano-Micro Lett. 13 (2021) 52. https://doi.org/10.1007/s40820-020-00565-4.

[75] J. KONG, S. YU, Fourier Transform Infrared Spectroscopic Analysis of Protein Secondary Structures, Acta Biochim. Biophys. Sin. (Shanghai). 39 (2007) 549–559. https://doi.org/10.1111/j.1745-7270.2007.00320.x.

[76] A. Rygula, K. Majzner, K.M. Marzec, A. Kaczor, M. Pilarczyk, M. Baranska, Raman spectroscopy of proteins: a review, J. Raman Spectrosc. 44 (2013) 1061–1076. https://doi.org/10.1002/jrs.4335.

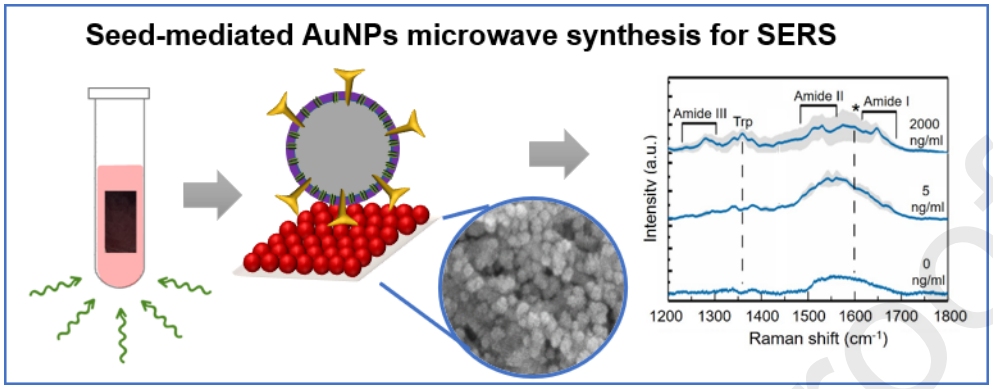

- Microwave-assisted seed mediated synthesis of AuNPs onto nanocellulose membranes;
- Citrate-based chemical route presents superior microwaves absorption for nanoparticles' synthesis;
- Rapid fabrication of nanocellulose-based SERS membranes by an in situ approach;
- Outstanding SERS membranes' shelf life up to 7 months;
- Successful spike protein screening from SARS-CoV-2 virus.

Credit Author Statement

A. C. M: Conceptualization, Methodology, Formal analysis, Investigation, Writing – Original Draft; T. P: Investigation, Writing – Review & Editing; M. M.: Investigation, Writing – Review & Editing; C. M.: Investigation; A. F. A.: Investigation; R. M.: Funding acquisition; M. G. F. S.: Supervision, Writing – Review & Editing; E. F: Supervision, Writing – Review & Editing, Funding acquisition